Hindawi
International Journal of Aerospace Engineering
Volume 2024, Article ID 8717164, 15 pages
https://doi.org/10.1155/2024/8717164

Research Article

A Dual-Hierarchy Synchronization Method for Signal Preambles with High Detection Rates for Satellite-Based ADS-B Receivers with Different Sensitivities

Xinhui Jian,[1] **Xuejun Zhang**,[1] **Jianxiang Ma**,[2] **and Weidong Zhang**[3]

[1]*School of Electronic Information Engineering, Beihang University, Beijing, China*
[2]*Big Data Division, Innovation Institute (Chengdu) of Beihang University, Chengdu, China*
[3]*School of Cyber Science and Technology, Beihang University, Beijing, China*

Correspondence should be addressed to Xuejun Zhang; zhxj@buaa.edu.cn

Received 17 March 2023; Revised 16 July 2023; Accepted 28 February 2024; Published 21 March 2024

Academic Editor: Chuang Liu

Existing methods are unable to achieve high detection rates and low false alarm rates of satellite-based Automatic Dependent Surveillance-Broadcast (ADS-B) signal preambles at extremely low signal-to-noise ratios (*SNRs*) using limited on-star resources. In this paper, a dual-hierarchy synchronization method is proposed, including a first-level coarse synchronization and a second-level fine synchronization. The coarse synchronization process involves three steps: (1) detection of unknown signals, (2) soft decision, and (3) adaptive interval output. The first step introduces the threshold (T_{MSED}) of the minimum signal energy to be detected to guarantee a high detection rate. In the soft decision step, a value (S_V) designed to improve the robustness of the system curbs false detection caused by noise interference. In the last step, the coarse synchronization interval radius (r) is mapped out according to the *SNR* to reduce resource consumption. The fine synchronization process is based on the coarse synchronization output, and the correlation peak is calculated to complete the synchronization of the signal preambles. The results show that the proposed method achieves a high detection rate of 96% at an extremely low *SNR* using a low sampling frequency of 10 MHz. Furthermore, the adjustment of T_{MSED} allows this method to be applied to ADS-B receivers with different sensitivities. The comprehensive performance of this method to achieve high detection rates and acceptable false alarm rates at extremely low *SNRs* with limited on-star resources is verified by final simulations to be superior to other methods.

1. Introduction

As the number of aircraft present in the airspace rapidly grows, the Automatic Dependent Surveillance-Broadcast (ADS-B) system is becoming a key surveillance tool for next-generation air traffic management due to its flexible surveillance mode and high-accuracy data-updating ability [1, 2]. However, the traditional ground-based ADS-B system cannot provide seamless global surveillance due to blind zones at ground stations [3]. In order to solve this problem, researchers have focused on satellite-based ADS-B systems to achieve real-time, continuous, and seamless surveillance globally [4–7].

The signal preamble detection of satellite-based ADS-B receivers is severely limited by extremely low signal-to-noise ratio (*SNR*) and fewer on-star resources [8], due to the fact that ADS-B systems were not originally designed for applications on satellites [9]. Several methods have been proposed to alleviate the various problems of signal detection that come with it. On the one hand, the initial detection of a 4-pulse preamble was used to judge the existence of the header and to calculate the arrival time of the signal, as was described in a previous study [10]. This method results in a low detection rate and a high false alarm rate due to the low *SNR* [11]. In order to make the false alarm rate acceptable, Ren et al. [12] proposed a novel preamble detection algorithm that follows four criteria: false alarm rate (CFAR) detection, deterministic symbol matching, consistent power testing, and null symbol validation. This method can guarantee a detection rate higher than 90% only if the *SNR* is not lower than 10 dB. However, the *SNR*s of satellite-based ADS-B signals are much lower than 10 dB based on the analysis of the communication link [5]. On the other hand, Qin and Yang [13] pointed out the importance of saving computational resources when processing signals on satellites. They designed a detection algorithm based on the preamble correlation to save resources. However, this method is not suitable for processing poorly correlated satellite-based ADS-B signal preambles. To obtain sufficient correlated information, Delovski et al. [14] directly detect signal frame headers at a high sampling frequency during intermediate frequency (IF). Although a detection rate of over 90% was achieved at a low *SNR*, the high sampling frequency of 105 MHz being used resulted in a significant increase in resource consumption. The application of this method is impractical on satellites with limited resources. Based on the above, the demand for a comprehensive algorithm that can robustly guarantee high detection rates and low false alarm rates at extremely low *SNRs* while consumes fewer on-star resources in satellite-based ADS-B signal detection attracts our attention.

We propose a dual-hierarchy synchronization method that incorporates three important steps: (1) detection of unknown signals, (2) soft decision, and (3) adaptive interval output. It enables the satellite-based ADS-B system to simultaneously meet the requirements of high detection rates, acceptable false alarm rates, fewer on-star resources consumed, and high robustness, even at extremely low *SNRs*. Our unique contributions are compared boldly and explicitly with the latest levels in Table 1 and further detailed as follows.

(1) We propose the first comprehensive synchronization method for extremely weak ADS-B signals that achieves high detection rates even at a low sampling frequency

(2) We introduce the threshold (T_{MSED}) of the minimum signal energy to be detected to achieve high detection rates at extremely low *SNRs*. This parameter can be adjusted to even ensure that the required detection rate is maintained for any ADS-B receiver with a different sensitivity

(3) We add a system robustness value (S_V) that not only reduces false alarm rates but also robustly handles adjacent ADS-B signals with different dynamic ranges

(4) We reduce the computational redundancy by mapping the relationship between the *SNR* and coarse synchronization interval radius (r) in addition to using a low sampling frequency

The first column of Table 1 represents the challenges faced in synchronization of satellite-based ADS-B signals, including extremely low *SNRs*, limited on-star resources, high detection rates, and low false alarm rates, with high robustness and strong applicability as additional advantages. The last column reflects which task of our method was used to address these challenges.

This paper is organized as follows. In Section 2, we build the mathematical model of the baseband signal of a satellite-based ADS-B system based on an analysis of the *SNR*. Section 3 describes the dual-hierarchy synchronization method for detecting satellite-based ADS-B signal preambles and the three key steps this method includes. In Section 4, the three important steps proposed in the method are simulated and validated. Furthermore, we also compared the simulation results with other methods in this section. The concluding remarks and potential future research topics are provided in the final section.

2. SNR and Mathematical Model of Digital Baseband Signals for Satellite-Based ADS-B

2.1. SNR Analysis of Baseband Signals. The sensitivity of the receiver is defined as the lowest signal energy required to ensure normal operation [15]. To determine the *SNR* of the baseband signal when the preamble is detected, we need to calculate the sensitivity of the satellite-based ADS-B receiver using the link budget without changing the transmitter power. L_d is the free-space propagation loss of the signal and is given by [16, 17]

$$L_d = 32.44 + 20 \lg R + 20 \lg F_c, \quad (1)$$

where R is the transmission distance of the signal in kilometer and F_c is the carrier frequency of the signal in megahertz. According to the actual situation [18, 19], we initially estimate that the vertical distance between the vehicle and satellite is R_{min}, and the farthest distance that the satellite can cover is R_{max}. The ADS-B signal carrier frequency is $F_c =$ 1090 MHz. By substituting the above values into (1), the L_d range can be estimated as $153\,\text{dB} \le L_d \le 164\,\text{dB}$.

Without changing the ADS-B transmitter power ($P_t = 53$ dBm), the received radio frequency (RF) power of the satellite-based ADS-B receiver can be obtained from

$$P_r = P_t + G_t + G_r - L_d - L_s, \quad (2)$$

where $G_t + G_r$ is the sum of the gain of the transmitting antenna and receiving antenna and L_s is the absorption loss caused by the atmosphere, rain, clouds, and fog in the carrier wave propagation process. By substituting these values of $G_t + G_r = 10\,\text{dB}$, $L_s = 1\,\text{dB}$, and $153\,\text{dB} \le L_d \le 164\,\text{dB}$ into (2), the peak power range of the satellite-based ADS-B receiver can be obtained as $-102\,\text{dBm} \le P_r \le -91\,\text{dBm}$. This range is consistent with the results of the simulated received signal described in the literature [5]. Thus, the system design and index allocation for the RF component and baseband signal processing component of the receiver should be based on this range.

The minimum peak power P_r is -102 dBm, and the duty cycle of pulse position modulation (PPM) is 50%, so the average power $P_{rV} = -102 - 3 = -105\,\text{dBm}$.

Table 1: Boldly contrasting our contributions to the relevant literatures.

Challenges	[10]	[12]	[13]	[14]	Our work	
SNR range for effective working① (dB)	≥4.5	≥10		≥0.4	≥0.4	Framework
Operating scenario of satellite-based ADS-B②						
High detection rates				✓	✓	Step 1
Acceptable false alarm rates		✓			✓	Step 2
Sampling frequency (MHz)	10	18	12.5	105	10	Framework
Fewer on-star resources consumed	✓	✓	✓		✓	Step 3
High robustness③					✓	Step 2
Strong applicability④					✓	Step 1

The ① shows that the method can achieve the basic requirement of 90% detection rate within this SNR range, where the SNR has been converted via (4) in Section 2.1. The ② describes a scenario which the sensitivity of the satellite-based receiver is as low as -102 dBm. Performance ③ represents whether the method can process signals with different dynamic ranges. Performance ④ indicates that the method can also be used for ADS-B receivers with different sensitivities. The last column shows the contributions of our work and the key ways in which they are being realized.

The noise of the receiver can be calculated using

$$P_{\mathrm{N}} = 10\lg(KTW) + \mathrm{NF}, \tag{3}$$

where K is the Boltzmann constant, the Kelvin temperature T is equal to 290 K, W is the bandwidth, and $\mathrm{NF} = -174$ dBm is the base noise of the receiver.

Assuming that the RF link has a receiver noise figure (RNF) of 2.5 dB and the bandwidth is 4 MHz [20], then the minimum SNR of the baseband signal for preamble detection can be expressed as

$$\mathrm{SNR}_{\min} = P_{\mathrm{rv}} - P_{\mathrm{N}} - \mathrm{RNF} = 0.479\ \mathrm{dB}. \tag{4}$$

This metric implies that the synchronization method for satellite-based ADS-B signals needs to achieve the desired performance at a SNR of 0.479 dB, including high detection rates, acceptable false alarm rates, fewer on-star resources consumed, and high robustness.

2.2. Mathematical Model of Digital Baseband Signals. The ADS-B signal has undergone PPM with 120 bits per signal and a duration of 120 microseconds. The energy of one bit can be defined using

$$E_{\mathrm{s}} = A^2 \times \frac{T}{2}, \quad T = 1\,\mu\mathrm{s}, \tag{5}$$

where A is the amplitude of the digital signal.

First, the preamble of the signal is composed of the initial 8 microseconds, and its corresponding position characteristic array is $m = [1, 0, 1, 0, 0, 0, 0, 1, 0, 1, 0, 0, 0, 0, 0, 0]$.

Then, the other 112 microseconds are data bits, which can be expressed as follows:

$$D = [d[1], d[2], \cdots, d[224]]. \tag{6}$$

These data bits have two forms that S_1 and S_2 can be represented using

$$\begin{cases} \text{If } S_1(k) = 1, k = 1, 2, \cdots, 112, \\ \quad d[2k-1] = 1, \\ \quad d[2k] = 0. \\ \text{If } S_2(k) = 0, k = 1, 2, \cdots, 112, \\ \quad d[2k-1] = 0, \\ \quad d[2k] = 1. \end{cases} \tag{7}$$

Finally, the position characteristics of one signal can be expressed as $B = [m\,D] = [b[1], b[2], \cdots, b[240]]$.

The unipolar pulse signal can be expressed as follows:

$$c(t) = A \sum_{k=1}^{240} b[k] g(t - kT_{\mathrm{B}}), \tag{8}$$

where $T_{\mathrm{B}} = 0.5\,\mu$s is the duration of a code element, $g(t)$ is a rectangular pulse, and $b[k] \in B$. The analog IF signal passing through the RF link is denoted as $e_{2\mathrm{ASK}}(t)$. The term $e_{2\mathrm{ASK}}(t)$ can be expressed as the product of the unipolar pulses and a sinusoidal carrier, as shown in

$$e_{2\mathrm{ASK}}(t) = c(t)\cos(\omega_{\mathrm{c}} t + \varphi_0) + \omega(t), \tag{9}$$

where $\omega_{\mathrm{c}} = 70$ MHz is the IF carrier corner frequency, φ_0 is the carrier initial phase (assumed to be 0), and $\omega(t)$ is the additive Gaussian white noise expressed as $\omega(t) = \omega_{\mathrm{c}}(t)\cos\omega_0 t + w_{\mathrm{s}}(t)\sin\omega_0 t$. With $e_{2\mathrm{ASK}}(t)$ as the input, the ADS-B digital baseband signal $y(n)$ is obtained following the processing steps outlined in Figure 1.

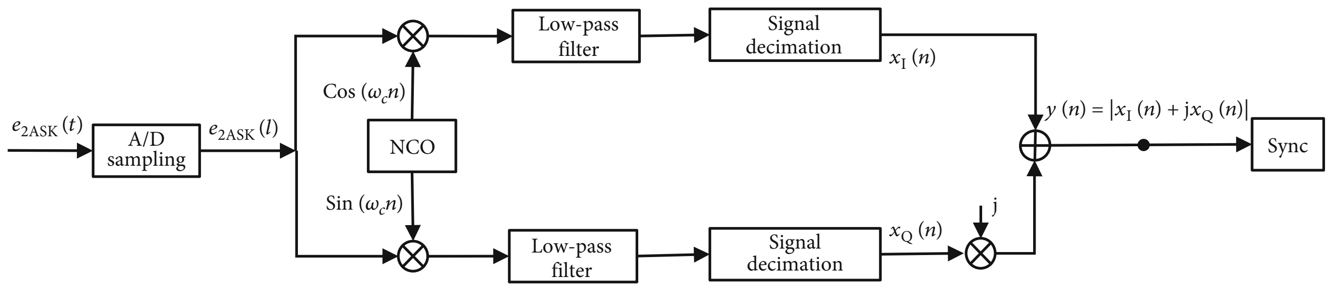

Figure 1: Digital baseband signal generation process.

As shown in Figure 1, with the sampling frequency $f_s = 10$ MHz, the digital IF signal $e_{2ASK}(l)$ can be obtained after conducting an analog-to-digital conversion. The signal can be expressed using

$$e_{2ASK}(l) = \frac{A}{\sqrt{2}} \sum_{k=1}^{240} b[k] g(lT_s - kT_B) \cos(\omega_c l T_B + \varphi_0) + \omega(lT_s), \tag{10}$$

where $T_s = 1/f_s = 0.01\,\mu$s.

First, $e_{2ASK}(l)$ is multiplied by the cosine and sine data generated by the numerically controlled oscillator (NCO).

Then, the obtained results are passed through low-pass filters and sampled to obtain the in-phase component $x_I[n]$ and the quadrature component $x_Q[n]$, as expressed in

$$\begin{cases} x_I[n] = \dfrac{A}{\sqrt{2}} \cos\varphi_0 \displaystyle\sum_{k=1}^{240} b[k] g'(n - kL) + \omega_I[n], \\ x_Q[n] = \dfrac{A}{\sqrt{2}} \sin\varphi_0 \displaystyle\sum_{k=1}^{240} b[k] g'(n - kL) + \omega_Q[n], \end{cases} \tag{11}$$

where $g'(n)$ is the discrete data of $g(lT_s)$ after filtering and sampling and $L = 5$ is the number of samples per code element.

Finally, $y[n]$ can be expressed as follows:

$$y[n] = \left| x_I + jx_Q \right|, \tag{12}$$

where the noise $\omega[n] = |\omega_I[n] + j\omega_Q[n]|$ satisfies $\omega \sim N(0, \sigma_n^2)$ based on Parseval's theorem [21, 22] and $\mathrm{SNR} = 10\,\lg(A^2 L/\sigma_n^2)$.

3. Proposed Dual-Hierarchy Synchronization Method

3.1. Design of the Dual-Hierarchy Synchronization Method. The dual-hierarchy synchronization method, which is performed by superimposing coarse synchronization on fine synchronization, is designed to overcome the detection rate problems associated with satellite-based ADS-B signals due to extremely low *SNR* and limited on-star resources. Figure 2 shows the operational framework for this method, and then, more detailed algorithms are described in Sections 3.2 and 3.3.

As show in Figure 2, after the coarse synchronization, the radius (r) of the interval in which the signal exists is calculated with a certain probability, and the position (*Position_Max*) corresponding to the maximum energy within that interval is obtained. Thus, a certain signal preamble is judged to fall in interval $S = [Position\_Max - r, Position\_Max + 120 \times 2L + r]$. Based on the S, the fine synchronization locates to the position (*P_Preamble*) of the signal preamble by filtering-matching and passes it to the next function to complete the signal preamble synchronization process [23]. The coarse synchronization plays the most important role in the proposed method and is the main contribution of this paper.

3.2. First-Level Coarse Synchronization Algorithm. The function of coarse synchronization is to find the approximate position of the signal preamble and output it to fine synchronization in the form of an interval. Its performance is required to achieve a high detection rate and a low false alarm rate. The challenge is the extremely low *SNR* of the signal and the limited resources available on the satellite. As shown in Figure 3, the coarse synchronization process consists of three main steps: the unknown signal detection in step 1, the soft decision in step 2, and the adaptive interval output in step 3. The first step is aimed at identifying the existence of the signals, the second step is responsible for extracting the complete signals, and the last step calculates the potential interval of the signal preamble. The details of each step are described as follows.

3.2.1. Step 1: Detection of Unknown Signals. In the detection of unknown signal step as shown in Figure 3, the energy accumulation of the signal is first described. The filter expression is $H = (h'[k])^T \times u[l]$, where $h'[k]$ satisfies $h'[240 - k] = [m, n]$, the array m is the preamble feature array as described in Section 2.2, and the array n is an all-one array with a length of 224. Because the number of samples of a single code element is $L = 5$, $u[l]$ is an all-one array of length L. For the matrix H with 5 columns and 240 rows, the elements of each row are reconstituted into an array $h[n]$ according to the row numbers in turn. By convolving $h[n]$ and $y[n]$, we can obtain the accumulation energy of one signal, as expressed by

$$z[j] = y[n] \otimes h[i], \tag{13}$$

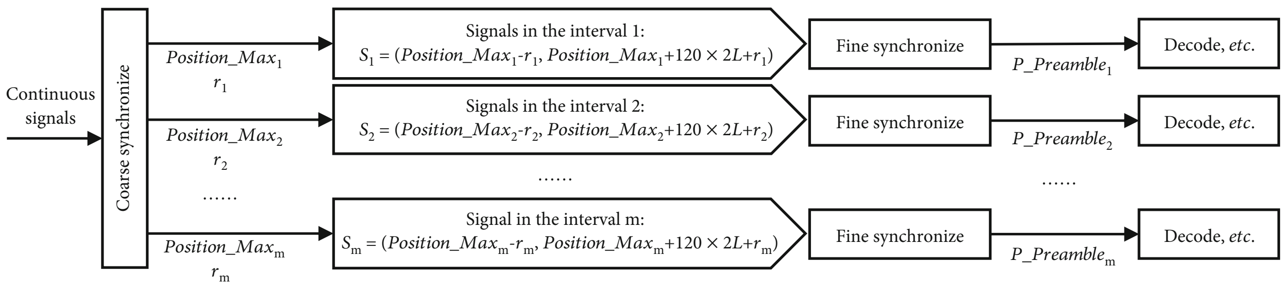

Figure 2: The operational framework of the dual-hierarchy synchronization method.

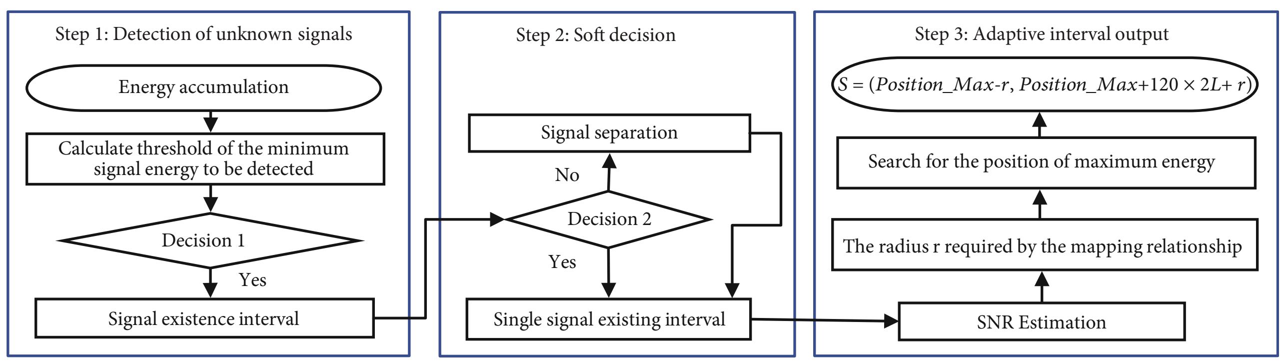

Figure 3: Coarse synchronization process.

where $y[n] = x_I^2[n] + x_Q^2[n]$ is the square of the amplitude of the signal with noise.

Because the ADS-B signal is modulated through PPM, the accumulated energy $z[j]$ can also be expressed using

$$z[j] = \sum_{j_1=1}^{l_1 L} z_1[j_1] + \sum_{j_0=1}^{l_0 L} z_0[j_0], \tag{14}$$

where l_0 and l_1 represent the number of low electrical level and high electrical level bits that have been convolved, respectively, and $l_1 L + l_0 L = j$. $\sum_{j_1=1}^{l_1 L} z_1[j_1]$ conforms to the noncentral chi-square distribution [24], and $\sum_{j_0=1}^{l_0 L} z_0[j_0]$ fits the central chi-square distribution [9]. When the signal preamble is fully synchronized, $l_1 = 116$ and $l_0 = 112$.

Then, the T_{MSED} term is introduced to determine whether a signal is present or not, as shown in

$$\begin{cases} z \geq T_{MSED}, H_1, \\ z < T_{MSED}, H_0, \end{cases} \tag{15}$$

where H_1 and H_0 represent the presence and absence of the signal.

When the energy accumulation length is sufficiently large (usually ≥30), according to the central limit theorem (CLT), the multiple independent random variables must obey the Gaussian distribution expressed as follows [25]:

$$z \sim \begin{cases} N\left(l_0\sigma_{\mathrm{n}}^2, 2l_0\sigma_{\mathrm{n}}^4\right), & H_0, \\ N\left(l_1\left(\sigma_{\mathrm{n}}^2 + \sigma_{\mathrm{s}}^2\right), 2l_1\left(\sigma_{\mathrm{n}}^2 + \sigma_{\mathrm{s}}^2\right)^2\right), & H_1. \end{cases} \tag{16}$$

Thus, the false alarm probability P_{f} and detection probability P_{d} are calculated as follows [26]:

$$\begin{cases} P_{\mathrm{f}} = P(z > T_{MSED} | H_0) = Q\left(\dfrac{T_{MSED} - l_0\sigma_{\mathrm{n}}^2}{\sqrt{2l_0\sigma_{\mathrm{n}}^4}}\right), \\ P_{\mathrm{d}} = P(z > T_{MSED} | H_1) = Q\left(\dfrac{T_{MSED} - l_1\left(\sigma_{\mathrm{n}}^2 + \sigma_{\mathrm{s}}^2\right)}{\sqrt{2l_1\left(\sigma_{\mathrm{n}}^2 + \sigma_{\mathrm{s}}^2\right)^2}}\right). \end{cases} \tag{17}$$

The T_{MSED} can be computed by (17), as shown in

$$T_{MSED} = Q^{-1}(P_{\mathrm{d}})\sqrt{2l_1\left(\sigma_{\mathrm{n}}^2 + \sigma_{\mathrm{s}}^2\right)^2} + l_1\left(\sigma_{\mathrm{n}}^2 + \sigma_{\mathrm{s}}^2\right), \tag{18}$$

where P_{d} can be obtained according to the system requirements. When the preamble of the signal is synchronized, $l_1 = 116$, $l_0 = 112$, and $\sigma_{\mathrm{s}}^2 = 10^{SNR_{\mathrm{min}}/10}\sigma_{\mathrm{n}}^2$. The SNR_{min} can be adaptively determined according to the receiver sensitivity, as described in Section 2.1. Thus, the T_{MSED} can be adjusted exactly to the needs of different situations. This is one of the advantages of this method: it is suitable for ADS-B signal receivers of different sensitivities. This parameter is verified in Section 4.1.

Finally, decision 1 is addressed using T_{MSED} and $z[j]$, as shown in Figure 3. This step is aimed at determining whether the accumulated energy $z[j]$ is greater than the T_{MSED} value based on (15). We delimit $z[j]$, which is continuously determined to be greater than T_{MSED}, within an interval defined as the signal existence interval (*SEI*). This result is passed to the step 2 (soft decision) as input.

3.2.2. Step 2: Soft Decision. Although the signal was judged to be present and the *SEI* was obtained, it is not possible to determine how many signals exist within this interval. The soft decision step is used to solve this problem and obtain the interval in which a single signal exists, denoted as *SSEI*. The key to this soft decision step is decision 2 as shown in Figure 3, which can be expressed in

$$\begin{cases} LengthSEI_m \geq S_V \times 120 \times 2L, \\ LengthSEI_m \leq 240 \times 2L, \end{cases} \tag{19}$$

where S_V is the value that guarantees the robustness of the system and $LengthSEI_m$ is the length of SEI_m.

If both inequalities in (19) are satisfied, the corresponding SEI_m is recognized as $SSEI_n$. The position corresponding to the maximum energy in $SSEI_n$ is recognized as $Position\_Max_n$. It will be passed on as output to the step 3 as shown in Figure 3.

If the second inequality is satisfied, but not the first, this means that this SEI_m is misclassified as a signal due to excessive noise. This detection should be abandoned. Therefore, S_V is important to reduce false alarms.

If the first inequality is satisfied but not the second, this means that, due to the filter length, this decision combines multiple signals shorter than 120 microseconds into the same signal interval. Thus, the signal separation described next is necessary.

The SEI_m must be separated dichotomously until (19) is satisfied, giving multiple single signal intervals $SSEI_n$. Assuming that the position corresponding to the maximum energy $z[Position\_Max_m]$ in SEI_m is $Position\_Max_m$, the signal separation rules are described as follows.

If $Position\_Max_m + 121 \times 2L \in SEI_m$, then

$$\begin{cases} SEI_{m'} = [SEI_m[1]: Position\_Max + 120 \times 2L], \\ SEI_{m'+1} = [Position\_Max + 120 \times 2L : SEI_m[\text{end}]]. \end{cases} \tag{20}$$

If $Position\_Max_m - 121 \times 2L \in SEI_m$, then

$$\begin{cases} SEI_{m'} = [\mathrm{SEI}_m[1]: Position\_Max - 120 \times 2L], \\ SEI_{m'+1} = [Position\_Max - 120 \times 2L : SEI_m[\text{end}]]. \end{cases} \tag{21}$$

Here, the $SEI_{m'}$ and $SEI_{m'+1}$ are the new intervals obtained by signal separation. These intervals must be again verified by decision 2 until multiple $SSEI_n$ are obtained.

3.2.3. Step 3: Adaptive Interval Output. Due to the presence of noise, there is a certain probability that $Position\_Max_m$ is not a true preamble [27]. Fine synchronization consumes many resources if the processing is performed using the whole *SSEI*. Based on these two factors, we have to provide a shorter fine synchronization interval where the signal preamble exists. The radius of this interval is noted as r, and the center point $Position\_Max_m$ remains the output of the previous step 2. Because the dispersion measures of the signal preambles differ among different *SNRs* [28], we establish a mapping relationship between the coarse synchronization-output interval r and *SNR*. The modeling details are explained in Section 4.3, and the mapping relationship is summarized in Table 2.

By estimating the *SNR*, r is obtained. Combined with $Position\_Max_m$, the more accurate interval of the signal preamble is transmitted to the fine synchronization level as shown in Figure 3, which is noted as $S = [Position\_Max - r, Position\_Max + 120 \times 2L + r]$.

3.3. Second-Level Fine Synchronization. To fully utilize the position characteristics of the signal preambles, the bipolar matching filter defined as $m' = [1,-1,1,-1,-1,-1,-1,1,-1,1,-1,-1,-1,-1,-1,-1]$ is chosen. The correlation coefficient (C) is obtained through a sliding correlation process using the output signal interval S of the coarse synchronization results and the filter m', as shown in

$$C = S \otimes m'. \tag{22}$$

When C is taken to be the maximum, the corresponding position is identified as the actual arrival point of the signal and is denoted as *P_Preamble*. At this point, the proposed synchronization method is completed with *P_Preamble* as the result.

4. Validation and Results

4.1. Simulation and Verification of T_{MSED}. As mentioned in the first step in Section 3.2, for ADS-B receivers with different sensitivities, high detection rates can theoretically be maintained by adjusting the T_{MSED}, which is one of the advantages of the dual-hierarchy synchronization method. It is necessary to simulate and verify the detection rates for different *SNRs* as in (17).

The first is a simulation of the operation of T_{MSED}. Assuming that the noise following a Gaussian distribution satisfies $w \sim \mathrm{N}(0, 10)$ and the system requires a detection rate of 96%, the T_{MSED} of ADS-B receivers with different sensitivities can be calculated using (18) (as drawn in Figure 4).

Figure 4 shows that when the receiver sensitivity is -102 dBm, the result of calculating the T_{MSED} is

$$T_{MSED} = Q^{-1}(P_d)\sqrt{2l_1(\sigma_n^2 + \sigma_s^2)^2} + l_1(\sigma_n^2 + \sigma_s^2) \approx 1891. \tag{23}$$

Table 2: Interval radius under different *SNRs*.

SNR (dB)	<0	[0,1)	[1,2)	[2,3)	≥3
Interval r	90	60	35	10	1

The r is the interval radius of the coarse synchronization output according to the different *SNRs*.

According to (23), the relationship between the *SNR* and the detection rate P_d can be expressed as

$$P_\mathrm{d} = Q\left(\frac{T_{MSED} - l_1\left(\sigma_\mathrm{n}^2 + \sigma_\mathrm{s}^2\right)}{\sqrt{2l_1\left(\sigma_\mathrm{n}^2 + \sigma_\mathrm{s}^2\right)^2}}\right), \quad (24)$$

where $l_1 = 116$ and $\sigma_\mathrm{n}^2 + \sigma_\mathrm{s}^2 = \left(1 + 10^{SNR/10}\right) \times 10$. This means that a receiver with a sensitivity of -102 dBm can achieve a detection rate of 96% by setting a threshold of $T_{MSED} = 1891$. This section will subsequently default the ADS-B receiver sensitivity to -102 dBm. Based on the above, the *SEI* can be obtained according to decision 1 in step 1 of Section 3.2, as shown in Figure 5.

In Figure 5, the solid blue line depicts the cumulative energy $z[j]$ of the signal in (14). The purple pentagram is the cumulative energy assuming only noise, which can be used as a reference.

T_{MSED} is indicated by the yellow line. Last, the orange dashed line depicts the *SEI* generated by the judgment of (15), which is the resulting H_1 set when z is greater than T_{MSED}.

Then, the verification process of the detection rate of this T is described. A Monte Carlo experiment was set up using MATLAB to verify the synchronization performance of the system under different *SNRs*. Based on the analysis in Section 2.1, ten thousand pieces of data were generated randomly when the *SNRs* satisfied $SNR(\mathrm{dB}) = [-0.521, 0.7479]$. The detection rates resulting from this method processing for $T_{MSED} = 1891$ are shown in Figure 6.

The blue line in Figure 6 represents the detection rates using the proposed method to process random data, and the red represents the theoretical one. The results justify the following conclusions. First, the detection rate reaches 95.98% when the *SNR* of the received signal is 0.479 dB. This result is almost consistent with (24). Secondly, the detection rates are all higher than 96% when the *SNRs* are higher than 0.479 dB and even reach 100% after the *SNRs* are higher than 3.479 dB. This proves that this method meets the requirement of high detection rate for satellite-based ADS-B systems. Thirdly, the processing results for signals with *SNRs* higher than 0.479 dB match the theory, but their results for signals with lower *SNRs* are worse than the theoretical values. This means that setting $T_{MSED} = 1891$ is well suited for receivers with a sensitivity of -102 dBm, while this parameter can be adjusted to apply to receivers with higher sensitivities. This also demonstrates the necessary study of the correlation between the T_{MSED} in this method and the sensitivity of the satellite-based ADS-B receiver.

4.2. Simulation and Verification of the Soft Decision Step. The power of the receiving signals is different because the satellite-based ADS-B system has different coverage. Furthermore, the decision 1 leads to false alarms due to the effect of noise. The minimum value of the S_V in (19) determines the false alarm rate, while its maximum value determines the maximum dynamic range of the signals that can be processed. This section will focus on verifying the robustness of the soft decision for processing signals with different dynamic ranges. The low false alarm rate will be verified in Section 4.4. The *SEI* may still satisfy (19) when two signals with high and low powers are adjacent to each other and their head-to-tail distance is less than the filter length. This phenomenon indicates the presence of more than one signal in this *SEI* (only the presence of two signals is considered here), as shown in Figure 7.

For the six signals shown in Figure 7, the signal powers are -95 dBm, -98 dBm, -95 dBm, -100 dBm, -95 dBm, and -102 dBm. The signals with powers of -95 dBm and -98 dBm are located in the same *SEI*, which is typical of those that need to be processed by step 2. We make the following assumptions. The system sensitivity is the minimum power p_2, and the maximum power p_1 of the signal that can be processed can be represented by the dynamic range $\exp^D$. The linear system is set up so that (25) is satisfied.

$$\exp^D = \frac{p_1}{p_2} = \frac{p_{\mathrm{B}1}}{p_{\mathrm{B}2}}, \quad (25)$$

where $p_{\mathrm{B}1}$ and $p_{\mathrm{B}2}$ are the powers of the baseband signals with RF signal powers p_1 and p_2, respectively.

We provide an example in Figure 8 to verify the effect of the S_V. Assume that the received RF signals are at powers of $P_1 = -95$ dBm (left) and $P_2 = -98$ dBm (right), that the time interval between them is $\Delta T = 30\,\mu s < 120\ \ \mu$s, and that the noise conforming to the Gaussian distribution satisfies $\omega \sim \mathrm{N}(0, 10)$, as shown in Figure 8(a). Since this interval is less than the length of the filter (1200 bits), these signals are often judged by (15) to be in the same *SEI*, as shown in Figure 8(c).

In Figure 8, since A_0 is the starting point for the convolution energy $z[j]$ of the signal $y[n]$ and the filter $h[i]$ in (13), it is noted as the coordinate origin. Point A_2 and point A_5 are used to assist in completing the signal separation. Point A_1 and point A_6 represent the intersections of the convolution energy $z[j]$ and the threshold T_{MSED}, which also denote the start and end points of the SEI_m. Therefore, we establish the following equation:

$$\begin{cases} x_1 p_{\mathrm{B}1} + T\sigma_\mathrm{n}^2 = T_{MSED}, \\ (3T + \Delta T - x_6) p_{\mathrm{B}2} + T\sigma_\mathrm{n}^2 = T_{MSED}, \end{cases} \quad (26)$$

where x_1 and x_6 are the horizontal coordinates of these two points, which also represent the distance the filter moves. The $p_{\mathrm{B}1}$ and $p_{\mathrm{B}2}$ are the baseband powers of the received signals, which can be expressed in terms of the *SNR* as $p_{\mathrm{B}1} = 10^{SNR_1/10}\sigma_\mathrm{n}^2$ and $p_{\mathrm{B}2} = 10^{SNR_2/10}\sigma_\mathrm{n}^2$, where $\sigma_\mathrm{n}^2 = 10$. Then, $T = 120\,\mu$s is the period length of the filter. When

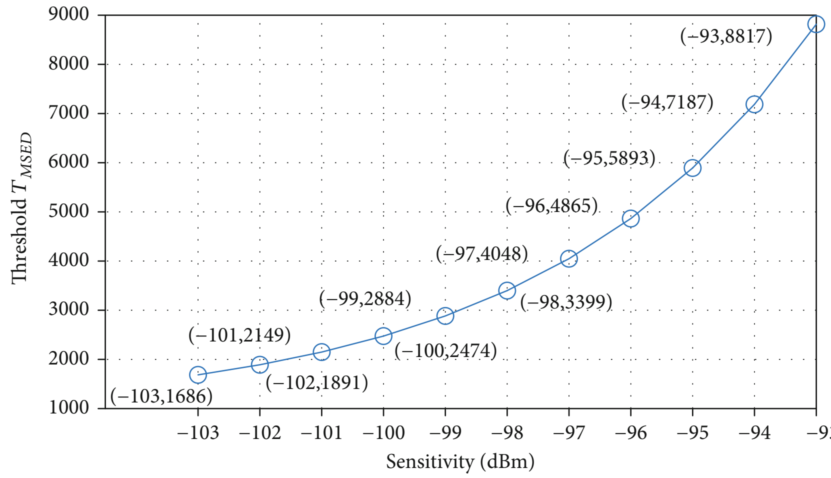

Figure 4: The T_{MSED} corresponding to ADS-B receivers of different sensitivities.

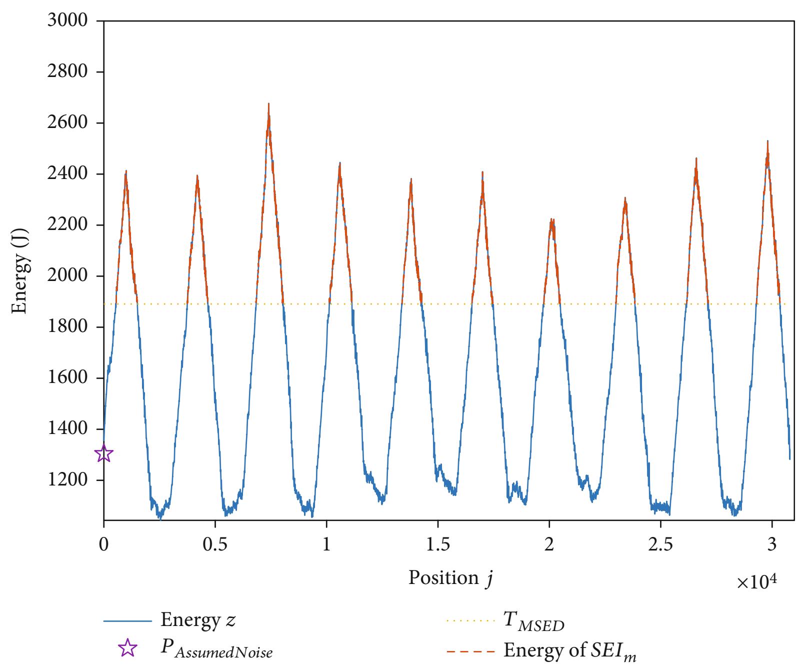

Figure 5: The *SEI* obtained after using the verdict of T_{MSED} on the cumulative energy $z[j]$ according to decision 1.

$T_{MSED} = 1891$, the x_1 derived from the first equation in (26) are listed in Table 3.

Assume that ΔT in (26) is set to zero, which is the limit of the soft decision; otherwise, the problem will turn into a solution interleaving. The x_1 and x_6 corresponding to signals of different received powers can be calculated using

$$x_1 = \frac{(3T + \Delta T - x_6)p_{B2}}{p_{B1}}, \Delta T = 0. \tag{27}$$

Furthermore, according to (19), we obtain

$$S_V T \le x_6 - x_1 \le 2T. \tag{28}$$

Combining (27) and (28) yields

$$S_V \le \frac{x_6 - (3T - x_6)p_{B2}/p_{B1}}{T} = \frac{x_6 - (3T - x_6)}{\exp^D \cdot T}. \tag{29}$$

Assume that the minimum power p_2 of the received RF signal is -102 dBm and the maximum power p_1 is -95 dBm. By combining Table 3 and (29), we can obtain

$$S_V \le 1.930. \tag{30}$$

Of course, if there is a requirement to process signals with a greater dynamic range, turning down the S_V can make this method applicable. This is one of the advantages

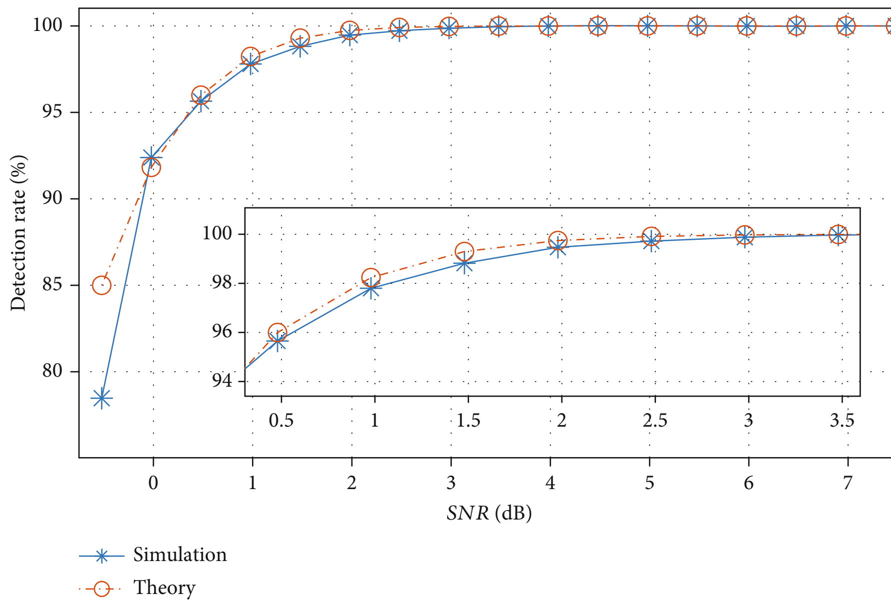

FIGURE 6: Theoretical and simulated detection rates obtained by the proposed method for signals with different *SNRs*.

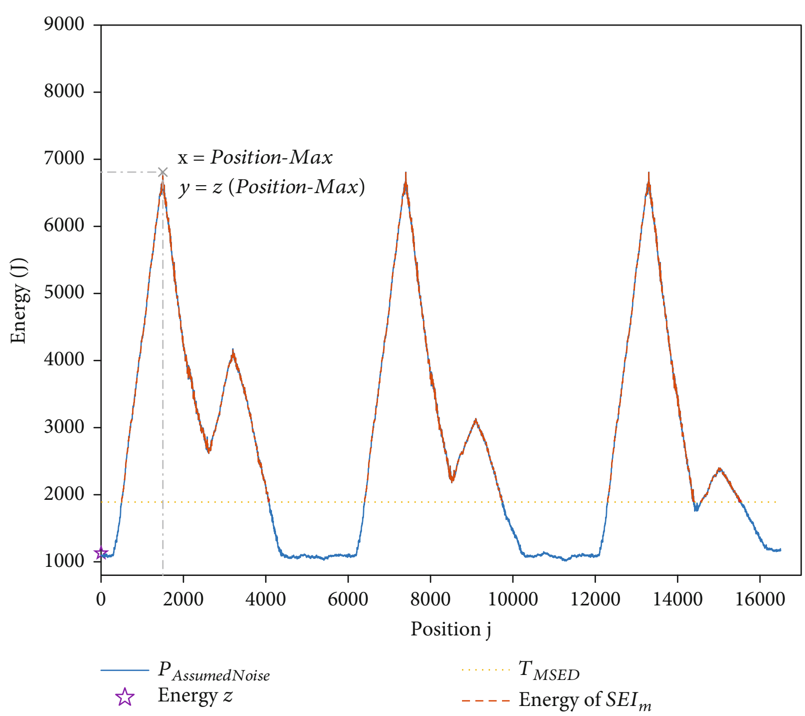

FIGURE 7: Schematic diagram of the *SEI* for signal separation under the T_{MSED} decision.

of the proposed method when applied according to the above scenario.

4.3. Simulation and Verification of the Adaptive Interval Output. According to the description of step 3 in Section 3, applying the adaptive interval derived based on the statistical detection criteria can reduce the computational effort because the length of the coarse synchronization interval output can be adjusted. The following two tasks will be done in this section. The first is to model the mapping relationship between the *SNR* and the adaptive interval output, which leads to the results in Table 2 in step 3 of Section 3.2. The second is to compare the effect on resource consumption before and after using the adaptive interval output through simulation experiments.

The first task reflects that the lengths of the adaptive output intervals $[Position\_Max - r, Position\_Max + r]$ differ under different *SNRs*. The model is built as follows. First

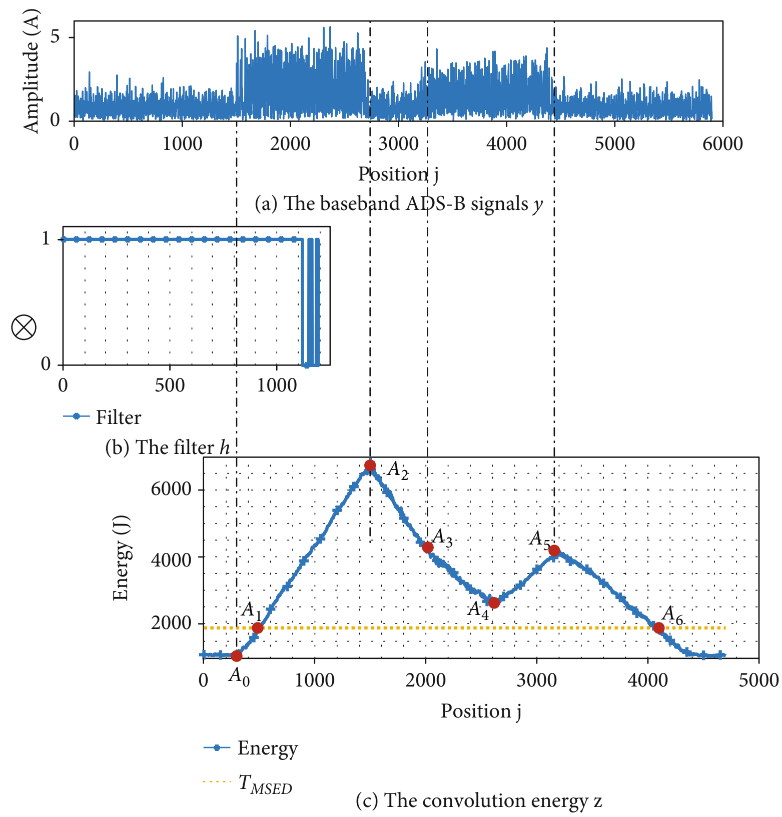

Figure 8: Situation before the soft decision step is applied to adjacent signals.

Table 3: Correspondences between the x_1 and the *SNRs*.

P (dBm)	-95	-96	-97	-98	-99	-100	-101	-102
SNR (dB)	7.479	6.479	5.479	4.479	3.479	2.479	1.479	0.479
x_1	12.3	15.5	19.6	24.6	31.0	39.0	49.2	61.9

The x_1 is the horizontal coordinate for the intersection of the energy curve and the T_{MSED}.

10,000 signal pieces are randomly generated of these seven *SNR* points (-2 to 4 dB with 1 dB step) using the Monte Carlo method. Then, the *Position_Max* value of each signal in the *SSEI* is determined for further use according to the method described in Section 3.2. Most critically, after continuously calculating the absolute distance (r) of each signal between the *Position_Max* and the known actual leading code position, the probability distribution of the r at each *SNR* point is statistically determined. Finally, the probability distributions of r for 10,000 signals at each *SNR* point are statistically shown in Figure 9. These probability statistic results also imply that the probabilities of *Position_Max* falling within the output interval of these *SNRs* should also satisfy the requirements of this method when the detection rate of the system is sufficiently high. Therefore, this probabilistic model is also called the "mapping of the *SNR* to the coarse synchronization interval output when the detection rate is satisfied."

The horizontal coordinate in Figure 9 indicates the absolute distance r of the *Position_Max* from the actual preamble position, and the vertical coordinate represents the probability that *Position_Max* falls within the range centered on the actual preamble with r as the radius. The orange line shows that if the required detection rate is 96% at a *SNR* of 1 dB, the corresponding horizontal coordinate r should be 35, which is the radius of the adaptive interval output of the coarse synchronization process. If the number of Monte Carlo experiments is sufficiently large, the curve is smoothed, and the test results are closer to the theoretical values. The corresponding r of the adaptive output interval derived under different *SNRs* at a detection rate of 96% are shown in Table 4.

The second task is to compare the resources consumed before and after the application of the above results. The five signals from 0 dB to 5 dB are generated separately based on MATLAB, and the effect achieved by step 3 is shown visually in Figure 10.

The orange lines in Figure 10 represent the SEI_m derived without any adaptive adjustment, and the black lines represent the coarse synchronization interval outputs $[Position\_Max - r, Position\_Max + r]$. As can be seen, the using of adaptive intervals significantly reduces the coarse synchronization

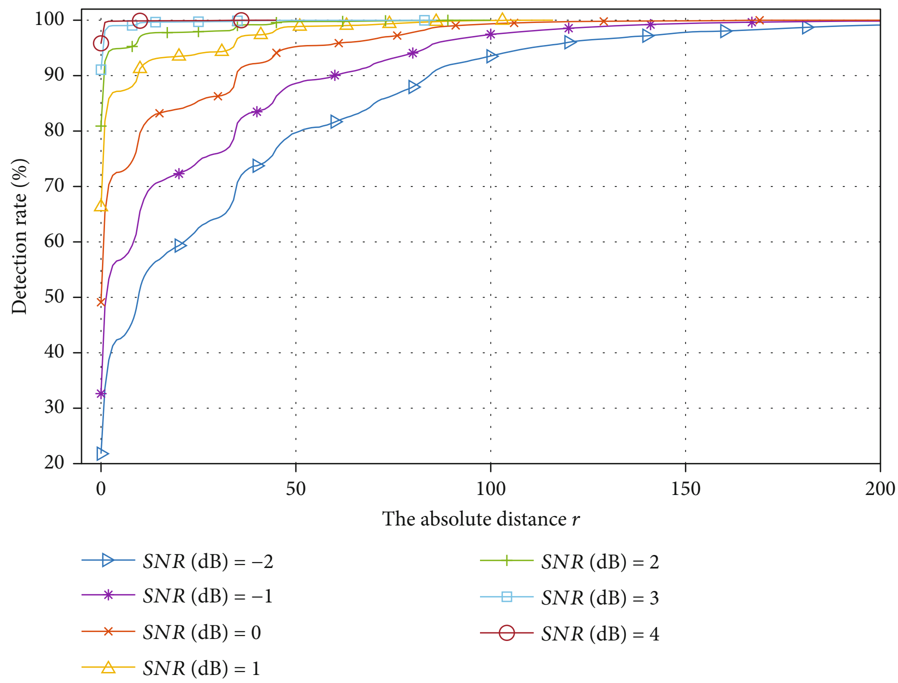

Figure 9: Mapping of the *SNR* to the coarse synchronization interval output when the detection rate is satisfied.

Table 4: Adaptive intervals in a simulation environment.

SNR (dB)	-2	-1	0	1	2	3	4
Detection rate (%)	96.02	96.07	96	96.69	96.98	98.1	99.6
r	120	82	60	35	10	1	1
Length of the adaptive interval	241	165	121	71	21	3	3

The detection rate is obtained by counting the detection results of 10,000 signals at a certain *SNR*; the r of the interval and the length of the adaptive interval are the conclusions obtained in step 3.

output. An example will be given below to quantify the amounts of resources saved.

A Monte Carlo experiment was used to randomly generate 10,000 signals with the received signal power of -102 dBm. At first, after processing using step 1 and step 2 described in Section 3.2, the probability distribution of the lengths of the *SSEI* was statistically calculated, as shown in Figure 11. The statistical average of these *SSEI* lengths is denoted as $AVE_{SSEI} = 850$. Finally, the coarse synchronization adaptive interval outputs are obtained using step 3. Comparatively, the probability distributions of these interval outputs were counted, and the results are presented in Table 5. The statistical average of these lengths can be calculated using

$$AVE' = \frac{\sum_m^N (2r_m + 1)}{N} \approx 144. \tag{31}$$

Combining the above statistics, the average lengths of the interval outputs before and after adaptive adjustment are 144 and 850, respectively. These results indicate that the application of step 3 reduces the computational burden by about 83.1% at a received RF signal power of -102 dBm, which is critical for resource-limited satellite systems.

4.4. Comparative Experiments and Results. Since several parameters of this method have been verified above, this section will compare the performances with reference to Table 1. Specifically, the first is the comparison of detection rate, the second is the comparison of resource consumption, and the third is the comparison of false alarm rate at the *SNR* for effective operation of the satellite-based ADS-B system. These comparison experiments will be performed based on the simulation conditions detailed below. Firstly, assuming that the powers of the received RF signals range from -102 dBm to -95 dBm, so the *SNRs* of the baseband signals obtained according to Section 2.1 range from 0.479 to 7.479 dB. Then, 10,000 baseband ADS-B signals are randomly and separately generated using the Monte Carlo method at each of these eight SNR points (0.479 to 7.479 dB with 1 dB step). Finally, these packets are used as homologous data for the comparison experiments described below.

The first is a comparison of the detection rates for each method. A detection rate of 96% is the requirement for the satellite-based ADS-B system to be popularized. The

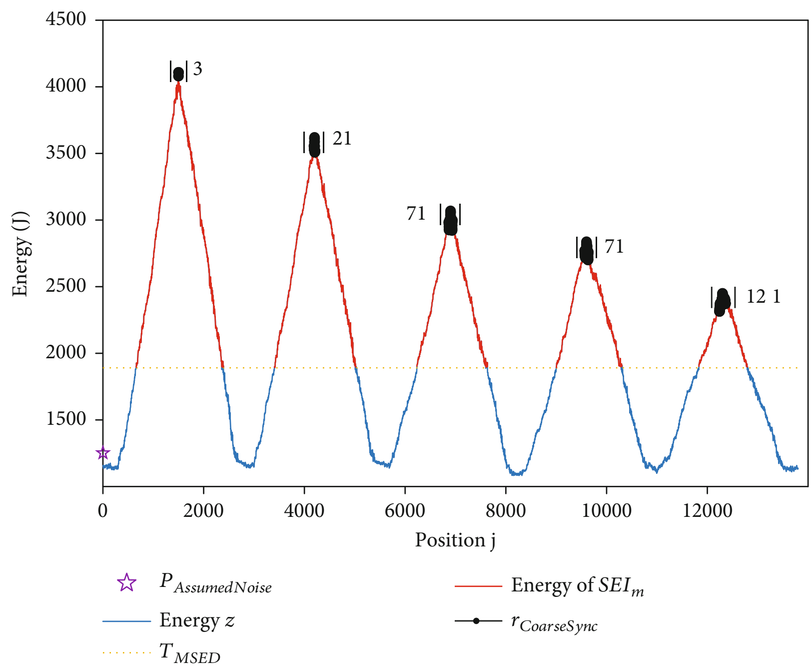

Figure 10: Comparison of the coarse synchronization output intervals derived before and after adaptation.

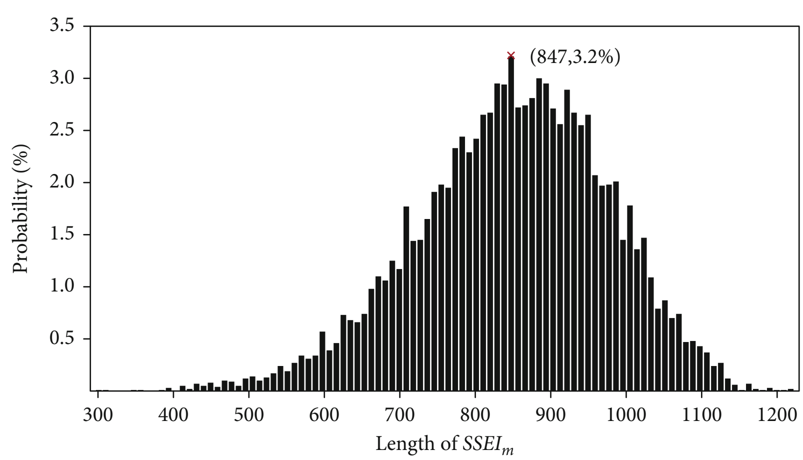

Figure 11: Probability distribution of the lengths of the *SSEIs* obtained before adaptive adjustment.

Table 5: Probability distribution of intervals after adaptive adjustment.

Length of the interval	71	127	165	241
Probability (%)	0.14	56.23	42.12	1.51

Probability of the lengths of adaptive intervals for 10,000 signals with a received power of -102 dBm.

detection rates of these signals were obtained separately using different experimental methods, such as four-pulse detection [10], multicriterion detection [12], coherent detection [14], and the proposed dual-hierarchy synchronization method. The results of these experiments are shown in Figure 12.

In Figure 12, the blue line represents the detection rates derived using the dual-hierarchy synchronization method. These detection rates were above 96% when the powers of the received RF signals were no less than -102 dBm. The green line shows the results of the four-pulse detection method [10] in a ground-based system, and the purple line represents the results of the multicriterion detection method developed by Ren et al. The detection rates of these two methods are both less than 96% when the powers of the received RF signals range from -102 dBm to -95 dBm [12]. The orange line represents the results of the coherent detection method proposed by Delovski et al. [14]. The detection rates of this method are similar to the results of our proposed method.

Then, the resource consumption should be compared due to the limited on-star resources. As presented in Section

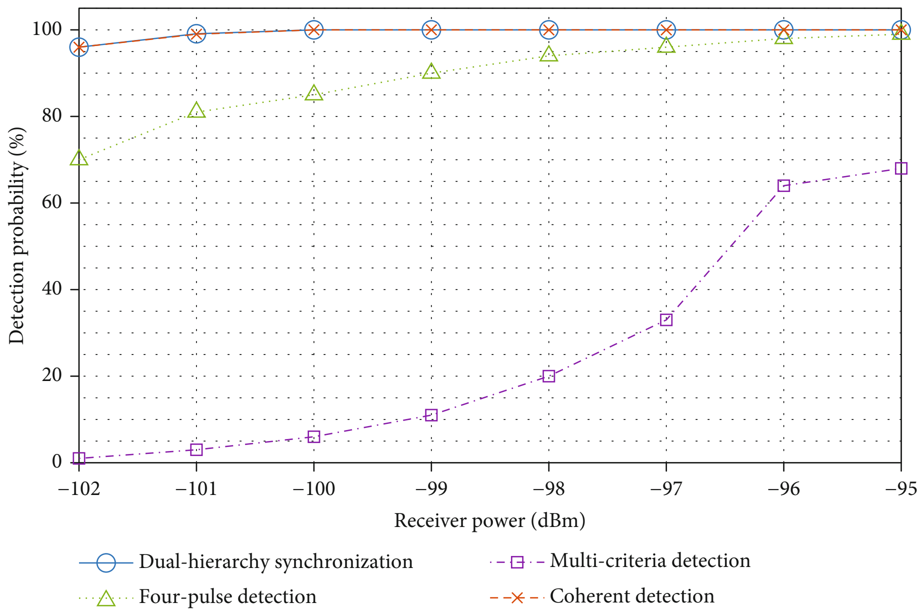

Figure 12: Detection rates for different methods obtained in simulation.

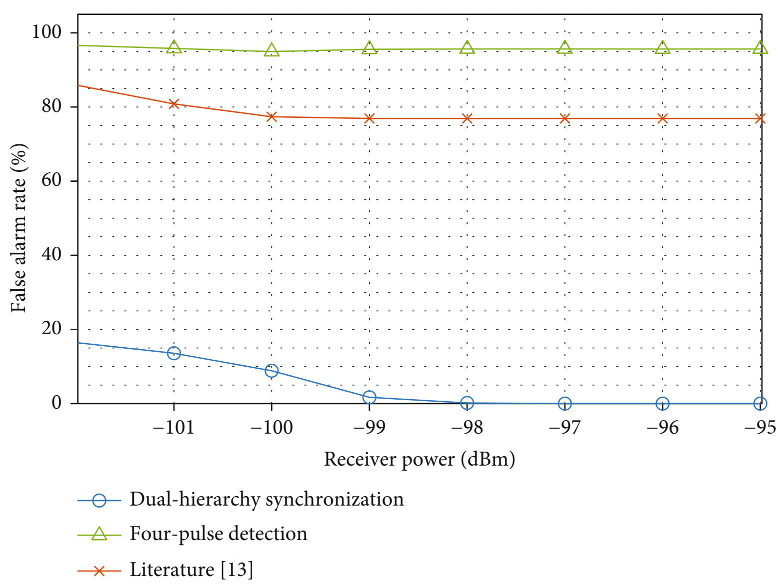

Figure 13: False alarm rates for different methods obtained in simulation.

1, the coherent detection in [14] was accomplished using a sampling frequency of 105 MHz for 112 data bits. Compared to other methods with sampling frequencies of 10 MHz, 12.5 MHz, and 18 MHz, this method consumes extremely large amounts of resources. Moreover, step 3 of our method reduces the resource consumption even further. Therefore, the coherent detection, which uses a lot of hardware resources in exchange for high detection rates, is not suitable for satellite-based ADS-B systems.

Finally, the suitability of the dual-hierarchy synchronization method for satellite-based ADS-B systems was assessed by determining whether its false alarm rate was acceptable. The detection rate of the method [12] using CFAR fails, although its false alarm rate is acceptable. The coherent detection [14], which does not have the false alarm rate taken into account, is defective. Therefore, using the homologous data described above, Figure 13 shows the false alarm rates for the literature [10, 13] and the proposed method.

The green and orange lines in Figure 13 represent the false alarm rates obtained by the methods of literature [10, 13], respectively. The blue line represents the false alarm rates obtained by the method proposed in this paper. Clearly, the results of our method are more satisfactory, with lower false alarm rates at low *SNRs* and near-zero false alarm rates at higher *SNRs*. This effect is accepted by satellite-based ADS-B systems.

In summary, only the dual-hierarchy synchronization method achieves such a comprehensive performance, which uses limited resources to achieve a detection rate of 96% with an acceptable false alarm rate at an extremely low *SNR*.

5. Conclusions

In this work, the *SNR* analysis for the baseband signal of the satellite-based ADS-B system in Section 2 is also applicable to satellites at other orbital altitudes. This section clarifies that the extremely low *SNR* is one of the difficulties in the synchronization of satellite-based ADS-B signal preambles. Another dilemma is the apparently limited on-star resources.

It is a challenge to achieve a high detection rate and a low false alarm rate with these two dilemmas.

Notably, the presented dual-hierarchy synchronization method can satisfy the detection rate requirements for signal preambles with limited resources at extremely low *SNR*. This cannot be achieved without the role of several important steps in Section 3.2. The T_{MSED} proposed in step 1 guarantees high detection rates at low *SNRs*, while providing value for strong applicability, and these results are verified in Section 4.1 and the first points of Section 4.4. The soft decision in step 2 guarantees low false alarm rates and can robustly handle signals with a high dynamic range. These results are verified in Section 4.2 and point 3 of Section 4.4. The use of a low sampling frequency and the mapping relations of step 3 both save on-star resources in varying degrees. These are demonstrated in Section 4.3 and the second part of Section 4.4, respectively. In summary, it is remarkable that this method achieves high detection rates and acceptable false alarm rates at extremely low *SNRs* with limited on-star resources, with such a comprehensive performance.

In addition, the proposed method utilizes only signal amplitude information and not signal phase information, allowing this method to avoid being affected by the Doppler frequency bias caused by high-speed satellite movements. However, if this phase information was effectively used for the coherent processing of the satellite-based ADS-B, it would improve the *SNR* of the baseband signal by 3 dB, and this would subsequently increase the probability of successful decoding the satellite-based ADS-B signal. Therefore, determining how to effectively use the phase information contained in satellite-based ADS-B signals is another likely area of improvement.

Data Availability

The data presented in this study are available on request from the corresponding author.

Conflicts of Interest

The authors declare that they have no known competing financial interests or personal relationships that could have appeared to influence the work reported in this paper.

Acknowledgments

This work is supported by the Ministry of Industry and Information Technology (No. 23100002022102001).

References

[1] M. Schafer, M. Strohmeier, V. Lenders, I. Martinovic, and M. Wilhelm, “Bringing up OpenSky: a large-scale ADS-B sensor network for research,” in *IPSN-14 Proceedings of the 13th International Symposium on Information Processing in Sensor Networks*, pp. 83–94, IEEE, Berlin, Germany, 2014.

[2] D. McCallie, J. Butts, and R. Mills, “Security analysis of the ADS-B implementation in the next generation air transportation system,” *International Journal of Critical Infrastructure Protection*, vol. 4, no. 2, pp. 78–87, 2011.

[3] J. Tang, “Review: analysis and improvement of traffic alert and collision avoidance system,” *IEEE Access*, vol. 5, pp. 21419–21429, 2017.

[4] P. Noschese, S. Porfili, and S. Di Girolamo, “ADS-B via Iridium NEXT satellites,” in *2011 Tyrrhenian International Workshop on Digital Communications-Enhanced Surveillance of Aircraft and Vehicles*, pp. 213–218, Capri, Italy, 2011.

[5] K. Werner, J. Bredemeyer, and T. Delovski, “ADS-B over satellite: global air traffic surveillance from space,” in *2014 Tyrrhenian International Workshop on Digital Communications-Enhanced Surveillance of Aircraft and Vehicles (TIWDC/ESAV)*, pp. 47–52, IEEE, Rome, Italy, 2014.

[6] B. G. Knudsen, M. Jensen, A. Birklykke et al., “ADS-B in space: decoder implementation and first results from the GATOSS mission,” in *2014 14th Biennial Baltic Electronic Conference (BEC)*, pp. 57–60, IEEE, Tallinn, Estonia, 2014.

[7] M. Strohmeier, M. Schafer, V. Lenders, and I. Martinovic, “Realities and challenges of nextgen air traffic management: the case of ADS-B,” *IEEE Communications Magazine*, vol. 52, no. 5, pp. 111–118, 2014.

[8] L. Zhang, “Development and prospect of Chinese lunar relay communication satellite,” *Space: Science & Technology*, vol. 2021, Article ID 3471608, 2021.

[9] P. Park and C. Tomlin, “Performance evaluation and optimization of communication infrastructure for the next generation air transportation system,” *IEEE Transactions on Parallel and Distributed Systems*, vol. 26, no. 4, pp. 1106–1116, 2015.

[10] RTCA, *DO-260B MOPS for 1090 MHz ES ADS-B and TIS-B*, RTCA, Washington, DC, USA, 2011.

[11] P. Ren, J. Wang, S. Yang, and H. Song, “A prototype of high-sensitivity noncoherent receiver for ADS-B signals,” *International Journal of Satellite Communications and Networking*, vol. 38, no. 4, pp. 341–354, 2020.

[12] P. Ren, J. Wang, H. Song, P. Zhang, and T. Ban, “A novel multi-criteria preamble detection algorithm for ADS-B signals,” *IEEE Access*, vol. 7, pp. 97319–97332, 2019.

[13] J. Qin and J. Yang, “Design and implementation of spaceborne ADS-B message detection algorithm,” in *DEStech Transactions on Engineering and Technology Research*, pp. 295–302, Shanghai, China, 2018.

[14] T. Delovski, J. Bredemeyer, and K. Werner, “ADS-B over satellite coherent detection of weak mode-S signals from low earth orbit,” in *The 4S Symposium 2016*, pp. 1–13, La Valetta, Malta, 2016.

[15] M. Tao, L. Zhou, H. Zeng, S. Li, and X. Liu, "50-Gb/s/λ TDM-PON based on 10G DML and 10G APD supporting PR10 link loss budget after 20-km downstream transmission in the O-band," in *Optical fiber communication conference*, pp. 1–3, Los Angeles, USA, 2017.

[16] L. E. Haro, G. J. Quiros, A. R. Villalba et al., "Hispa Sim: a web application for satellite link budget optimization and management," in *2017 11th European Conference on Antennas and Propagation (EUCAP)*, pp. 3295–3299, IEEE, Paris, France, 2017.

[17] A. Nauman and M. Maqsood, "System design and performance evaluation of high altitude platform: link budget and power budget," in *2017 19th International Conference on Advanced Communication Technology (ICACT)*, pp. 138–142, IEEE, Pyeongchang, Kwangwoon Do, South Korea, 2017.

[18] M.-S. Huang, R. M. Narayanan, Y. Zhang, and A. Feinberg, "Tracking of noncooperative airborne targets using ADS-B signal and radar sensing," *International Journal of Aerospace Engineering*, vol. 2013, Article ID 521630, 12 pages, 2013.

[19] O. Kodheli, E. Lagunas, N. Maturo et al., "Satellite communications in the new space era: a survey and future challenges," *IEEE Communication Surveys and Tutorials*, vol. 23, no. 1, pp. 70–109, 2021.

[20] Y. Hemaltha, R. Kumar, M. Mendhe, and B. N. Kumar, "Design & implementation of activity detection based configurable receiver architecture for EW application," in *2015 IEEE MTT-S International Microwave and RF Conference (IMaRC)*, pp. 113–115, IEEE, Hyderabad, India, 2015.

[21] P. Stoica, P. Babu, and J. Li, "New method of sparse parameter estimation in separable models and its use for spectral analysis of irregularly sampled data," *IEEE Transactions on Signal Processing*, vol. 59, no. 1, pp. 35–47, 2011.

[22] S. S. Nuza and A. Z. Mazrekaj, "Link budget analysis in the network designed mobile WiMAX technology in the territory of the urban area of the city of Gjakova," *International Journal of Computer Science Issues*, vol. 9, no. 5, pp. 357–360, 2012.

[23] C. Yue, T. Huo, M. Lu et al., "A systematic method for constrained attitude control under input saturation," *IEEE Transactions on Aerospace and Electronic Systems*, vol. 59, no. 5, pp. 6005–6015, 2023.

[24] A. F. Siegel, "The noncentral chi-squared distribution with zero degrees of freedom and testing for uniformity," *Biometrika*, vol. 66, no. 2, pp. 381–386, 1979.

[25] Y. Miao, G. Yang, and L. Shen, "The central limit theorem for LS estimator in simple linear EV regression models," *Communications in Statistics-Theory and Methods*, vol. 36, no. 12, pp. 2263–2272, 2007.

[26] B. Le, Z. Liu, and T. Gu, "Chaotic oscillator and other techniques for detection of weak signals," *IEICE Transactions on Fundamentals of Electronics, Communications and Computer Sciences*, vol. 88, no. 10, pp. 2699–2701, 2005.

[27] M. K. Simon, *Probability distributions involving Gaussian random variables: a handbook for engineers and scientists*, Springer, New York, 2002.

[28] B. Kosko and S. Mitaim, "Robust stochastic resonance: signal detection and adaptation in impulsive noise," *Physical Review E*, vol. 64, no. 5, article 051110, 2001.